https://doi.org/10.5194/egusphere-2025-4283
Preprint. Discussion started: 30 September 2025

Limited influence of bedrock strength on river profiles: the dominant role of sediment dynamics

Nanako Yamanishi[1] and Hajime Naruse[1]

[1]Division of Earth and Planetary Science, Graduate School of Science, Kyoto University, JP

Correspondence: Nanako Yamanishi (yamanishi.nanako.23r@st.kyoto-u.ac.jp)

Abstract. Bedrock river incision is a fundamental process driving the evolution of mountainous landscapes. Bedrock strength is often considered a primary control on incision rates and river profile morphology, with laboratory experiments showing a strong correlation between erosion rate and tensile strength. However, in natural settings, lithological boundaries frequently do not correspond to changes in the channel gradient. This study addresses this apparent paradox by integrating field observations with numerical experiments in the tributaries of the Abukuma River basin, northeastern Japan. Field surveys were conducted to measure bedrock tensile strength, riverbed gravel grain size, and the spatial distribution of lithologies. Despite more than an order-of-magnitude variation in bedrock tensile strength across the study area, the channel slopes remained nearly uniform. Numerical experiments were performed using three models of bedrock river erosion to investigate the underlying mechanisms. Among them, the sediment-flux-dependent model, which explicitly incorporates sediment cover and tool effects, most accurately reproduced the observed longitudinal profiles. The results reveal that local lithology does not directly influence channel slope due to a negative feedback between sediment cover and river gradient. Increased erodibility reduces slope, which enhances sediment cover and suppresses further erosion, thereby offsetting the impact of bedrock strength. These findings highlight the limited role of bedrock strength in controlling channel gradients and underscore the importance of sediment dynamics, particularly sediment supply and grain size, in shaping fluvial topography. Future research should explore how lithology-dependent variations in sediment characteristics influence river profile development.

1 Introduction

Bedrock river incision driven by fluvial processes plays a fundamental role in shaping mountainous landscapes (Whipple, 2004; Howard, 1994). This incision results from a combination of processes, including weathering, abrasion by saltating particles, plucking, cavitation, and debris scouring (Whipple et al., 2013; Campforts et al., 2020). While channel slope and drainage area have long been recognized as key controls, recent studies emphasize the importance of additional factors such as bedrock lithology, sediment grain size, and sediment supply (Sklar and Dietrich, 2001, 2004). Given the complexity of these controls, researchers have increasingly turned to river profiles to reconstruct signals of past climate change and crustal uplift (e.g., Molnar and England, 1990; Pritchard et al., 2009).

Among the various controls on river incision, bedrock strength has often been assumed to exert a strong influence on erosion rates. Laboratory experiments have shown that incision rate can scale with the square of tensile strength (Sklar and Dietrich,

https://doi.org/10.5194/egusphere-2025-4283
Preprint. Discussion started: 30 September 2025

2001), and recent field-based studies have highlighted its role in landscape evolution. For example, Haag et al. (2025) demonstrated a strong correlation between rock strength, erosion rate, and topography in southeastern Brazil. These results suggest that the mechanical properties of bedrock should be a critical control on river incision.

However, empirical observations of actual river longitudinal profiles often contradict this expectation. Even in regions where the bedrock tensile strength varies by more than an order of magnitude, the local channel gradients remain remarkably uniform. In theory, under steady-state conditions where erosion balances uplift, lower bedrock erodibility should result in steeper slopes to maintain the incision. Conversely, studies such as Hayakawa and Oguchi (2009) report that variations in bedrock strength do not necessarily coincide with changes in the channel gradient, challenging the predictive power of rock strength alone.

One explanation for this paradox is the sediment cover effect, which may play a more dominant role than rock hardness in regulating bedrock incision (Sklar and Dietrich, 2004; Sklar and Dietrich, 2006). Bedrock rivers commonly erode via the sediment tool effect, where moving clasts abrade the channel bed. However, this process is only effective when the sediment supply is sufficient to provide tools but not so abundant that the bed becomes completely covered. When cover becomes extensive, it shields the bedrock surface from direct impacts, thereby suppressing erosion rates. Guryan et al. (2024) demonstrated that models incorporating sediment cover yield more accurate predictions of river profiles, emphasizing the need to account for sediment dynamics.

Despite the growing recognition of the significance of the sediment cover effect, field-based quantification remains challenging. Although there are several attempts in the field measurements on the sediment cover rate under fair-weather conditions (Johnson et al., 2009; Carr et al., 2023), observations typically capture conditions during low flow. In contrast, most bedrock incisions occur during rare, high-energy floods; thus, the measured sediment cover may not represent that during active erosion. Indeed, experimental studies by Fernández et al. (2019) indicated that transient, fluctuating sediment cover—rather than mean cover—governs the erosion potential, especially near the transitions between exposed and covered bedrock. Such temporal dynamics are difficult to capture through field snapshots alone. Therefore, numerical modeling is essential for evaluating the spatial and temporal variability of the sediment cover and its geomorphic consequences (Sklar and Dietrich, 2006; Beer et al., 2017). Despite this understanding, relatively few studies have quantitatively examined the combined influence of bedrock strength and sediment cover on actual river profiles using direct measurements of rock strength.

This study aims to fill this gap by conducting systematic measurements of the bedrock tensile strength in multiple tributaries of a bedrock river system and by using these data to inform the numerical models. We evaluated three numerical models that represent varying levels of complexity in their treatment of erosion processes: the sediment-flux-dependent model (SFDM), the area-based stream power model (ASPM), and the stream power model with alluvium conservation and entrainment (SPACEM). Among these, only SFDM explicitly accounts for the sediment tool effect, while ASPM considers only the bedrock strength. SPACEM incorporates both the bedrock strength and the sediment cover, but not the tool effect explicitly. By applying these models to field data, including measurements of grain size and bedrock strength, we conducted simulations to assess how well each model reproduces the observed river topography. Our goal is to clarify how the relationship between the bedrock strength and the channel slope changes with or without the sediment cover effect, and which physical parameters are most essential for accurately capturing the longitudinal profile of bedrock rivers.

https://doi.org/10.5194/egusphere-2025-4283
Preprint. Discussion started: 30 September 2025

2 Geologic and Topographic settings

This study investigated the tributaries of the Abukuma River near the Koriyama City in Fukushima, Japan (Fig. 1 (a)). The Abukuma River drains the Nakadori area in Fukushima, covering 5,400 km^2 and being 239 km in length. The study area is about 150 km from the river mouth, located in the west of the Koriyama City. Five tributaries, Takinosawa, Hisawa, Fukazawa, Sangasawa, and Gohyaku River, were surveyed. Four of these tributaries (Takinosawa, Hisawa, Fukazawa, and Sangasawa) join Gohyaku River, which merges into the mainstream of the Abukuma River (Fig. 1 (c), Tab. 1). These rivers are all bedrock rivers partially covered with gravel.

The study area is in the forearc region of the Northeastern Japan Arc, which is bounded by the Tanakura tectonic line from the Southwestern Japan Arc (Ichikawa, 1990). A gentle synclinal structure with an NNE-SSW trending fold axis exists in this area, where the strata dip 20°–40° in the maximum. Several North-South trending faults are distributed in this study, while they are not active faults (Kubo et al., 2003; Yamamoto and Sakaguchi, 2023).

The bedrock of the study area is composed of metamorphic rocks, the Cretaceous igneous rocks, the Middle Miocene sedimentary rocks, and the Late Miocene pyroclastics with volcanic rocks. The metamorphic rocks are the muscovite-biotite-plagioclase-quartz gneiss, distributed in the central region of the study area. Their formative age is unknown. The Lower Cretaceous Abukuma granitic rocks, consisting of the granodiorite (Kubo et al., 2003) in the surveyed area, are distributed in the northern region of the study area. The Middle Miocene Horiguchi Formation, consisting of marine sedimentary rocks, is distributed in the southwestern region of the study area (Yamamoto and Sakaguchi, 2023). Massive sandstones and alternating beds of parallel-laminated sandstones and siltstones occur in this formation. The Late Miocene Kogyoku Formation is composed mainly of pyroclastic flow deposits filling the Kogyoku Caldera distributed in the northeastern region of the study area (Yamamoto and Sakaguchi, 2023). Dacite, lapilli tuff, and tuff breccia occur in the Formation. In addition to these formations, intrusive dacites and andesites occur in both igneous and sedimentary sequences.

The uplift and denudation rates of the drainage basin of the Abukuma River were quantified using various methods. From the coastal and river terrace surfaces formed along the mainstream, Fujiwara et al. (2005) estimated the average uplift rate of this basin as 0–0.3 m yr^{-1} (Fujiwara et al., 2004) for the recent 100,000 years. Apatite and zircon (U-Th)/He thermochronometry also suggested the denudation rates of this region. Fukuda et al. (2020) applied this method to the Cretaceous granitic rocks in the Abukuma mountain area, estimating that it is about 0.01 mm yr^{-1}.

The erosion rate was also estimated using terrestrial cosmogenic nuclides formed near the bedrock surface. Matsushi et al. (2014) measured denudation rates in the Abukuma Mountains using terrestrial cosmogenic nuclides and concluded that the denudation rate is 0.076–0.124 mm yr^{-1}. In summary, most of the results agreed that the denudation rates of the drainage basin of the Abukuma River are relatively slow (less than 0.3 mm yr^{-1}), compared with the denudation rates ranging from 0.1 to 1 mm yr^{-1} in the Ou Backbone Range, the central region of the Northeastern Japan Arc (Fukuda et al., 2020).

https://doi.org/10.5194/egusphere-2025-4283
Preprint. Discussion started: 30 September 2025

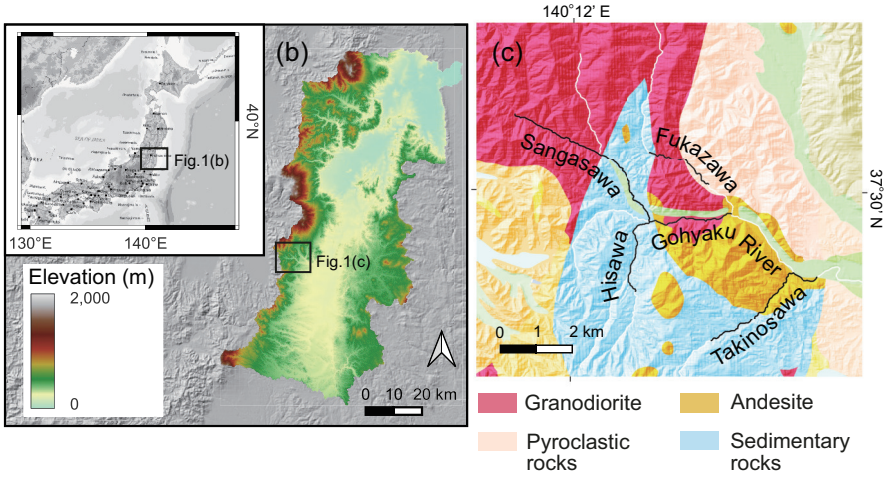

Figure 1. Index map and surveyed areas. The map data were obtained from Technical Report of the Geospatial Information Authority of Japan. (a) Location of the Abukuma River basin. (b) Map of the Abukuma basin. The topographic elevation is exhibited in colors. (c) Geological map with surveyed tributaries.

Table 1. Tributary information. Takinosawa, Hisawa, Fukazawa, and Sangasawa are tributaries of Gohyaku River.

Name	Length (km)	Drainage Area (km^2)
Takinosawa	5.2	7.4
Hisawa	5.3	8.9
Fukazawa	8.4	13.7
Sangasawa	5.6	17.5
Gohyaku River	25.9	190

3 River incision model

Numerous bedrock incision models have been proposed not only to understand the formative mechanisms of the bedrock river profiles (e.g. , Sklar and Dietrich, 1998; Whipple and Tucker, 1999; Sklar and Dietrich, 2004; Inoue et al., 2014; Aubert et al., 2016) but also to estimate the crustal uplift rates of mountainous regions (e.g. , Howard, 1994; Pritchard et al., 2009; Roberts et al., 2012). In those models, the following formulation was utilized to represent bedrock river elevation change in the continuous uplifting area:

$$\frac{\partial \eta}{\partial t} = U - E \tag{1}$$

where η denotes bedrock elevation, U and E are the uplift and bedrock erosion rates, respectively. In the steady state, the left side of Eq. (1) equals zero, and thus the erosion rate balances with the uplift rate.

https://doi.org/10.5194/egusphere-2025-4283
Preprint. Discussion started: 30 September 2025

Among various incision models, this study examined the sediment-flux-dependent model (SFDM) and two types of stream power models (Sklar and Dietrich, 2004; Chatanantavet and Parker, 2009; Inoue et al., 2017; Campforts et al., 2020; Guryan et al., 2024) to evaluate their appropriateness to account for the actual responses of the bedrock rivers to differences in bedrock strength. SFDM (Sklar and Dietrich, 2004; Whipple and Tucker, 2002) focuses on the abrasion-saltation process as the dominant mechanism of bedrock incision (Sklar and Dietrich, 2004). This model considers that the flux of the impact kinetic energy of transported sediment particles determines the incision rate. The stream power models consider that the bedrock incision rates are proportional to the loss of the stream energy per unit time and area (i.e., stream power) (Howard, 1994). The formulations of these models are described in detail below.

3.1 Sediment-flux-dependent model

In the sediment-flux-dependent model (Sklar and Dietrich, 2004), the incision rate E [m s^{-1}] is obtained by:

$$E = V_i I_r (1 - P_c) \tag{2}$$

in which V_i is the average volume of bedrock detached per particle impact, I_r is the rate of particle impacts per unit area per unit time, and P_c is the fraction of the covered riverbed.

Regarding the bedrock as an elastic brittle material, V_i can be rewritten by the classic impact wear model of Bitter (1963) as:

$$V_i = \frac{1/2 M_p (U_i \sin\alpha)^2}{\varepsilon_v} \tag{3}$$

where M_p [kg] denotes particle mass. U_i [m s^{-1}] indicates particle impact velocity, and α is saltation impact angle. The parameter ε_v [J] denotes the total energy required to erode a unit volume of rock (Sklar and Dietrich, 2004). The threshold energy ε_v is calculated by (Engle, 1978; Sklar and Dietrich, 2001):

$$\varepsilon_v = \frac{k_v \sigma_t^2}{2Y} \tag{4}$$

where σ_t [MPa] is bedrock tensile strength, and k_v denotes rock resistance coefficient. Y [MPa] represents Young's modulus. By substituting Eq. (4) into Eq. (3), we obtain:

$$V_i = \frac{\pi \rho_s D_s^3 w_{si}^2 Y}{6 k_v \sigma_t^2} \tag{5}$$

where ρ_s [kg m^{-3}] and D_s [m] denote the density of sediment and the diameter of a spherical sediment grain, respectively. $M_p = \rho_s \pi D_s^3 / 6$ is the mass of a spherical grain, and w_{si} [m s^{-1}] is the vertical component of the particle velocity on impact (i.e., $w_{si} = U_i \sin\alpha$)

Here, the number of particle impacts per unit time and area I_r is proportional to the flux of the bedload particles and inversely proportional to the downstream distance between the impacts. Using the sediment flux volume per unit width q_s [m^2 s^{-1}] and the saltation hop length L_s [m], I_r is expressed as:

$$I_r = \frac{\rho_s q_s}{M_p L_s} = \frac{6}{\pi D_s^3} q_s \frac{1}{L_s} \tag{6}$$

https://doi.org/10.5194/egusphere-2025-4283
Preprint. Discussion started: 30 September 2025

Substituting Eqs. (5) and (6) into Eq. (2), bedrock incision rate E is recast as:

$$E = \frac{\rho_s w_{si}^2 Y}{L_s k_v \sigma_t^2} q_s (1 - P_c) \tag{7}$$

Chatanantavet and Parker (2009) proposed that the abrasion coefficient can be defined as:

$$\beta = \frac{\rho_s w_{si}^2 Y}{L_s k_v \sigma_t^2} \tag{8}$$

Using this formulation, Eq. (7) can be rewritten as:

$$E = \beta q_s (1 - P_c) \tag{9}$$

Based on the flume experiments in the field scale, Inoue et al. (2014, 2017) pointed out that the erosion rate is proportional to the square root of the grain size rather than the shear stress and that it does not significantly depend on the Young's modulus. From this experimental result, Inoue et al. (2017) proposed the following relation:

$$E = \beta_0 \sigma_t^2 \left(\frac{D_s}{k_s} \right)^{0.5} q_s (1 - P_c) \tag{10}$$

where β_0 is an empirical coefficient (0.0001) [kg^{2}m^{-3}s^{-4}], k_s [m] represents the hydraulic roughness height, which is determined by the equation $k_s = \kappa_a P_c + \kappa_b (1 - P_c)$. Here, κ_a is a roughness coefficient that is linear to the grain diameter D_s, and κ_b is a constant representing the bedrock roughness. We adopted this relation in the model calculation.

The bedrock covered ratio P_c can be expressed in various ways; however, in this study, it is defined as

$$P_c = \frac{q_s}{q_t} \tag{11}$$

following the work of Sklar and Dietrich (2004). The sediment transport capacity q_t [m^2 s^{-1}] takes the form (Luque and and, 1976):

$$q_t = 5.7 (R_b g D_s^3)^{1/2} (\tau^* - \tau_c^*)^{\frac{3}{2}} \tag{12}$$

R_b denotes the nondimensional buoyant density of the sediment ($R_b = (\rho_s - \rho_w)/\rho_w$). The parameters ρ_w [kg m^{-3}] and g [m s^{-2}] denote the water density and gravity acceleration, respectively. The Shields stress τ^*, which is the nondimensional bed shear stress, is defined as:

$$\tau^* = \frac{\tau_b}{(\rho_s - \rho_w) g D_s} \tag{13}$$

where τ_b is the bed shear stress. The critical Shields number τ_c^* is the value of τ^* at the threshold of particle motion, which was regarded as constant (0.03) for simplicity.

Assuming that the stream flows in a uniform steady condition, the bed shear stress τ_b is calculated as:

$$\tau_b = \rho_w C_f^{1/3} g^{2/3} \left(\frac{Q_w}{W} \right)^{2/3} S^{2/3} \tag{14}$$

https://doi.org/10.5194/egusphere-2025-4283
Preprint. Discussion started: 30 September 2025

where C_f denotes the bed friction coefficient. Q_w [m^3 s^{-1}] and W [m] represent the water discharge and the width of the river, respectively. S indicates the bed slope.

Water discharge Q_w is determined by the following equation (Whipple and Tucker, 1999):

$$Q_w = k\bar{P}A \tag{15}$$

where k is a discharge coefficient representing rainfall variability, and $\bar{P}$ [m s^{-1}] denotes the average precipitation per unit area. A [m^2] represents the drainage area. Because the amounts of precipitation causing bedrock erosion are expected to be significantly larger than the average condition, the discharge coefficient k is also expected to be considerably greater than unity.

Assuming that the bedload sediment supply from the tributaries of the stream is proportional to the volume of the eroded material in the drainage area, the bedload discharge per unit width q_s domain is obtained as:

$$q_s(x) = \frac{1}{W(x)}\left(q_s(0)W(0) + a\int \frac{dA}{dx}E(x)dx\right) \tag{16}$$

where x [m] is the streamwise distance from the upstream end of the calculation domain, and $q_s(0)$ is the bedload sediment supply at the upstream end. The ratio of the bedload to the total sediment supply is represented by a.

The sediment supply per unit width at the upstream end is assumed to be in a steady state, where the erosion rate E_{eq} is equal to the uplift rate of the bedrock. The bedload sediment discharge $q_s(0)$ at the upstream end ($x = 0$) is written as:

$$q_s(0) = \frac{kA(0)E_{eq}}{W(0)} \tag{17}$$

where $A(0)$ and $W(0)$ denote the drainage area and the channel width at the upstream end, respectively.

The channel width W is estimated by the empirical formulation using the river discharge (Finnegan et al., 2005) as follows:

$$W = k_w Q_w^{0.5} \tag{18}$$

where k_w is the uniquely determined coefficient for each tributary.

To calculate the steady-state ($E = U$) channel profiles, Eq. (10) was recast to solve for the channel slope S using Eqs. (1), (12), (13), and (14), which takes the form:

$$S_{\mathrm{eq,SFDM}} = \left[\frac{R_b g^{1/3} D_s}{C_f^{1/3}(Q_w/W)^{2/3}}\left\{\tau_c^* \right.\right. \tag{19}$$

$$\left.\left. + \left(\frac{\beta_0 q_s^2}{5.7(R_b g)^{1/2} D_s(\beta_0 D_s^{1/2} q_s - k_s^{1/2}\sigma_t^2 U)}\right)^{2/3}\right\}\right]^{3/2} \tag{20}$$

3.2 Stream power models

We applied two types of the stream power model. One is the Area-based Stream Power Model (ASPM), which considers the lithologic strength of bedrocks (Campforts et al., 2020). This model does not account for the effect of the sediment cover rate on the river bed. The other is the Stream Power with Alluvium Conservation and Entrainment Model (SPACEM), which considers both the lithologic strength and the sediment cover rate (Guryan et al., 2024).

https://doi.org/10.5194/egusphere-2025-4283
Preprint. Discussion started: 30 September 2025

The ASPM is represented by the following equation:

$$E = k_a L_E S^n A^m \tag{21}$$

where k_a (m^{1-2m} yr^{-1}) is the erosional efficiency parameter excluding the influence of the lithological erodibility, and L_E is the relative lithological erodibility index. The positive exponents m and n are empirical parameters depending on lithology, rainfall variability, and sediment load (Campforts et al., 2020; Whipple and Tucker, 1999). The erosional efficiency k_a was determined by the Bayesian optimization in this study. L_E was determined using the value proposed in Campforts et al. (2020).

On the other hand, the SPACEM considers both the lithology and the sediment cover rate, but does not consider the sediment tool effect. This model considers the rates of erosion E_r and entrainment E_s, which relate to the sediment thickness on the riverbed. The following equation represents the erosion rate E_r:

$$E_r = K_r q_w S^n e^{-H/H_*} \tag{22}$$

where K_r is the bedrock erodibility, q_w is the water discharge per unit width ($= Q_w/W$), H is the thickness of the sediment cover, and H_* is the bedrock roughness scale. K_r reflects the bedrock strength. The entrainment rate of the sediment from the bed E_s is represented as:

$$E_s = K_{sed} q_w S^n (1 - e^{-H/H_*}) \tag{23}$$

where K_{sed} denotes the sediment erodibility. In this model, the cover ratio P_c is determined as H/H_*. The sediment thickness H depends on the rate of sediment entrainment E_s and deposition D_s, so that the relationship is calculated as:

$$(1-\phi)\frac{\partial H}{\partial t} = D_s - E_s = \frac{q_s}{q_w} W_s - E_s \tag{24}$$

where ϕ and q_s denote the sediment porosity and the sediment flux per unit width, respectively. W_s is the grain settling velocity determined by the grain size D_s. In this study, q_s, q_w was calculated using Eq. (16), (15).

Assuming the steady-state ($E = U$), the channel slopes can be calculated in the same manner as SFDM:

$$S_{\mathrm{eq,SPACEM}} = \left(\frac{q_s W_s}{K_{sed} q_w^2} + \frac{U}{q_w K_r} \right)^{1/n} \tag{25}$$

In this calculation, the grain settling velocity W_s was assumed to be spatially constant in this model.

The value of K_r for the most fragile rock type (i.e., tuff) was set to 1.0×10^{-5} according to (Guryan et al., 2024). Assuming that this coefficient is proportional to the rock tensile strength, the bedrock erodibility $K_{\mathrm{r},i}$ for the ith rock type was determined as follows:

$$K_{\mathrm{r},i} = \frac{\sigma_{\mathrm{t},i} K_{\mathrm{r,tuff}}}{\sigma_{\mathrm{t,tuff}}} \tag{26}$$

where $\sigma_{t,i}$ and $\sigma_{\mathrm{t,tuff}}$ denote the tensile strengths of the ith rock type and tuff, respectively.

3.3 Optimization of model parameters

In this study, the discharge coefficient k and channel width coefficient k_w were optimized to minimize the elevation differences between the actual river profile and the result of the model calculation. The objective function was defined as the root mean square (RMS) of the total elevation differences summed over the 5 tributaries.

$$RMS = \sqrt{\frac{1}{NM} \sum_{n,m=1}^{NM} (z_{nm}^O - z_{nm}^C)} \tag{27}$$

https://doi.org/10.5194/egusphere-2025-4283
Preprint. Discussion started: 30 September 2025

Table 2. A list of optimized parameters and their searched ranges.

model	params	range
SFDM	k	0–150
	k_w	0–15 (channel specific value)
ASPM	k_a	0–15
SPACEM	k	0–15

z^O_{nm} and z^C_{nm} represent the observed and calculated elevation, respectively. The optimal parameters were determined using Optuna, which is an optimization framework based on Bayesian optimization, a method that efficiently explores the optimal solution by sequentially updating the posterior distribution based on the evaluation results of a probabilistic model.

This study performed the Bayesian optimization with 10,000 trials to fit the model outputs to the observed river longitudinal profiles. As a result, the optimal parameters were obtained: k and k_w for SFDM, k_a for ASPM, and k for SPACEM. In the case of SFDM, k_w was individually optimized for each tributary, while the remaining parameters were treated as common values across all tributaries. The search ranges for these parameters are summarized in Table 2. Note that the uncertainties associated with the optimized parameters were not explicitly evaluated in this analysis.

4 Methods for topographic and geologic analysis

4.1 Topographic analysis

The topographic elevation, slope, and drainage area along the channels of the surveyed rivers were extracted from the digital elevation model (DEM) of the Geospatial Information Authority of Japan. First, 10-m-mesh DEM data of the surveyed tributaries were utilized to calculate the flow accumulation. The Deterministic 8 algorithm, where each pixel is assumed to flow in the maximum dip direction, was employed to obtain the drainage areas (O'Callaghan and Mark, 1984). The pixels exceeding 7×10^4 pixels in the drainage areas were regarded as river channels. The channel slope was then calculated along the channel path from the elevation data. The geographical information system software SAGA GIS was used for these procedures (Conrad and Böhner, 2015).

The normalized steepness index k_{sn} was used to clarify the effect of the bedrock strength on the channel steepness in all the investigated tributaries. This parameter is defined as the upstream area-weighted channel gradient (Campforts et al., 2020; Wobus et al., 2006):

$$k_{sn} = SA^{\theta} \tag{28}$$

The exponent θ is the concavity index, which is generally set to 0.45 (Wobus et al., 2006).

A chi plot is often used to identify whether the river profile is in the steady-state, or not (Perron and Royden, 2013). It is a coordinate transformation to linealize the river profile determined by:

$$\chi = \int_{X_b}^{X} \left(\frac{A_0}{A(x)} \right)^{m/n} dX \tag{29}$$

where X is the distance from downstream, and x_b is a base level. A_0 denotes a reference drainage area, and the drainage area at the downstream end is set in this study.

https://doi.org/10.5194/egusphere-2025-4283
Preprint. Discussion started: 30 September 2025

4.2 Measurement of Rock Strength

The lithologies of the bedrocks were distinguished by the naked eye in the field survey and were recorded in the geological route map of the researched tributaries. The 1:50,000 and 1:200,000 geologic maps published by the Geological Survey of Japan were also used to distinguish the lithologies where the bedrocks were not exposed on the channels.

Then, the tensile strengths of the bedrocks of the representative lithologies were sampled and measured using the Brazilian tension splitting test (Vutukuri et al., 1974). Before the analysis, the specimens were submerged in the water under a vacuum condition for 12 weeks until their weight did not change. This procedure is to measure the bedrock strength in the wet condition because it has been shown that the water saturation condition affects the rock tensile strength (Bao et al., 2021).

In this test, the specimens had a diameter of 50 mm and a length of 25 mm (Society, 2016). The load was applied to the specimen at 1 μm s^{-1} until a crack formed, and the maximum load P_{max} [kN] at the moment of failure was measured.

The tensile strength σ_t was then determined using the following Eq. (30).

$$\sigma_t = \frac{2P_{max}}{\pi DL} \times 1000 \tag{30}$$

where D (mm) and L denote the diameter and length of the specimen, respectively.

The gneiss measured in this study had a schistosity plane, and the measurement values can exhibit large variability depending on the surface on which the failure occurred. We assumed that the riverbed failure occurred along the weak plane, so we adopted not the average value, but the value when the specimen was cropped along the weak plane.

4.3 Automated grain size measurements of riverbed gravels

The grain sizes of the riverbeds were measured from the 3D point cloud data taken by the drone (Steer et al., 2022). The measurement procedures were as follows. (1) The drone (DJI Air-2s) photographed approximately 100–200 m^2 areas of the riverbeds. (2) The 3D point clouds exhibiting riverbed surface morphologies were produced by the Structure from Motion algorithm using the Agisoft Metashape. (3) The triaxial ellipsoid fitted the morphology of each gravel to measure grain diameter using the software G3Point (Steer et al., 2022).

This study defined the representative grain diameter $\bar{D_s}$ as the mean of the diameter of the spheres in the weighted arithmetic mean (D_{50}), which are equal to the fitted tri-axial ellipsoids in volume.

Since the G3Point program can analyze a maximum of 1 million points at a time, this study split the analysis area into two or three non-overlapping rectangular regions with a width of 5 m or less, and the mean values of these subareas were used as the measurement result of the surveyed area. We cropped the water surface contained in the 3D point cloud manually because G3Point sometimes misidentified the water surface as the grain surface.

To estimate the mean diameter D_s of the riverbed gravels along each stream, the measured values were interpolated with Sternberg's law Eq. (31) (Sternberg, 1875):

$$D_x = D_0 \exp(-\alpha_d x) \tag{31}$$

where D_0 is the grain diameter at the origin, and α_d is the change rate of the mean diameter. This study assumed that the river gravels fine downstream so that α_d is supposed to be a positive value. These parameters D_0 and α_d were estimated using the least-squares method.

The grain sizes of the riverbed gravels were also measured manually at the two locations (Sakura River and Gohyaku River) to evaluate the accuracy of the automated measurements. In this manual measurement, the longest (a), intermediate (b), and short (c) axes were measured, and the results were compared with those obtained by the G3Point program.

https://doi.org/10.5194/egusphere-2025-4283
Preprint. Discussion started: 30 September 2025

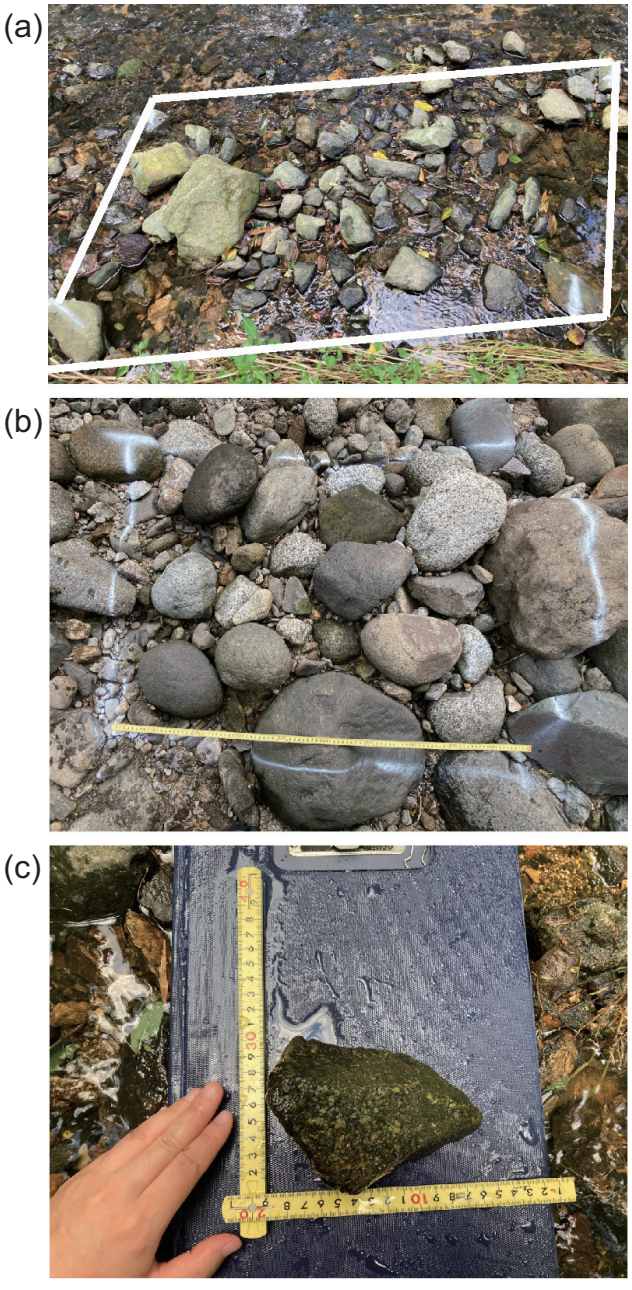

Figure 2. Photos of river gravels. (a) Photograph of gravels at Sakura River, the Tamura-Country, Fukushima. The area surrounded by the white lines was about 1.0×2.5 m. (b) Photograph of gravel at Gohyaku River, the Koriyama City, Fukushima. The area size was 0.8 m×1.0 m. (c) Manually measuring the gravels.

https://doi.org/10.5194/egusphere-2025-4283
Preprint. Discussion started: 30 September 2025

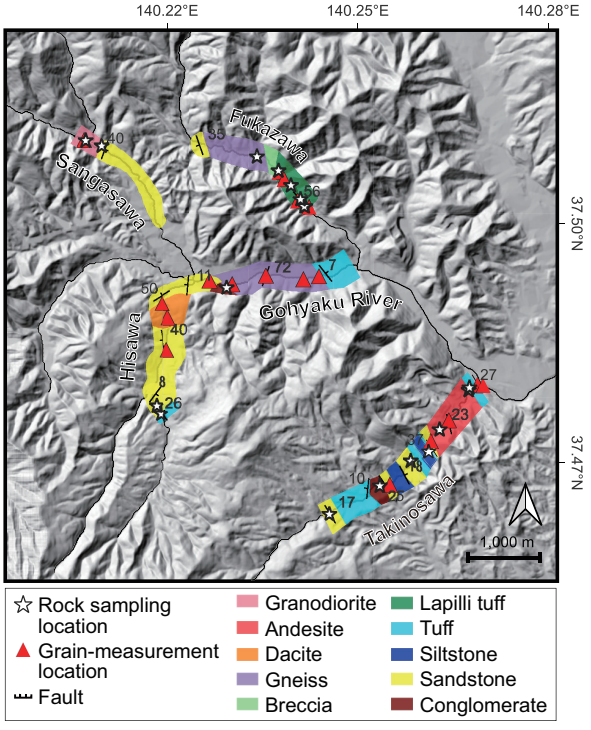

Figure 3. Route map in the researched area. The data of lithologic distributions in the unsurveyed areas were referred from previous studies (Kubo et al., 2003; Yamamoto and Sakaguchi, 2023). The star mark represents the location of the rock sampling. The pink triangle represents the location where the grain size distributions were measured using the drone. DEM data was obtained from Technical Report of the Geospatial Information Authority of Japan.

5 Results

5.1 Topography and geology of the surveyed channels

We identified ten types of sedimentary, pyroclastic, gneiss, and igneous rocks exposed on the riverbed of five tributaries of the Abukuma River (Takinosawa, Hisawa, Fukazawa, Sangasawa, and Gohyaku Rivers). The sedimentary rock is subdivided into conglomerate, massive sandstone, and siltstone. The pyroclastic rock includes volcanic breccia, lapilli tuff, and tuff. The igneous rocks are granodiorite and andesite. The volcanic and pyroclastic rocks are distributed in the northeastern region where Takinosawa and Fukazawa exist. The granodiorite is exposed in the northwestern region (Sangasawa). A major fault exists in the upstream region of Gohyaku River. A gentle synclinal structure with an NNE-SSW trending fold axis was observed in the study area, whereas an anticlinal structure was also observed upstream of Takinosawa and a further south tributary. These clinal structures were all trending NNE-SSW.

The result of topographic analysis and geological survey indicated that the river profiles did not vary significantly in slope at the lithologic boundaries. Figure 4 exhibits the channel longitudinal profiles of the surveyed tributaries extracted from the DEM, and the lithologies

https://doi.org/10.5194/egusphere-2025-4283
Preprint. Discussion started: 30 September 2025

identified through the field surveys were plotted as the symbols and colors. Most of the rivers have weakly concave-downward smooth profiles. The channel slopes in the surveyed region range from 0.02 to 0.05.

Several knickpoints can be observed in Sangasawa, Fukazawa, and Gohyaku River, but they do not correspond to the lithologic boundaries. The knickpoints in Fukazawa and Gohyaku River are located in the range where the gneiss is distributed. A small knickpoint is also observed in the middle of Sangasawa. This point corresponds to the significant change in the drainage area of the river, while the lithologic boundary between the granodiorite and sandstone is located slightly downstream of this knickpoint.

The check dams were located in Hisawa and Sangasawa. The knickpoint downstream of Hisawa coincides with the location of the check dam. No significant topographic change at the fault was observed in the field.

The chi-plot results (Fig. 5) did not show typical knickpoints that correspond to all tributaries. Takinosawa has a knickpoint that is absent in other tributaries. The steepness of Takinosawa, Hisawa, and Gohyaku River over $\chi = 20,000$ was almost the same; on the other hand, that of Fukazawa and Sangasawa was much steeper.

5.2 Bedrock strengths

The measured results of the bedrock strengths indicated that igneous and metamorphic rocks exhibited significantly larger tensile strength than sedimentary rocks (Fig. 3; Tab. 3). The strengths of igneous and metamorphic rocks ranged from 4.3 to 8.2 MPa. The dacite at Fukazawa demonstrated the maximum tensile strength of 8.2 MPa, which was more than 18 times larger than the minimum tensile strength of tuffs (0.46 MPa). The sedimentary rocks ranged in tensile strength from 0.4 to 2.4 MPa. They demonstrate variation in their strength depending on the location. The sandstones along Takinosawa were harder than those along Sangasawa.

The correlation between channel slope and bedrock tensile strength was weak, with an R^2 value of 0.061. The channel slope slightly increased, along with an increase in tensile strength. The range of channel slope at each tensile strength was large.

5.3 Grain size distribution along river channels

5.3.1 Comparison between automated and manual measurements

The median grain size of riverbed gravels automatically measured by the G3Point closely matched well with manual measurements (Fig. 7). The median grain size was 0.21 m for automated measurements and 0.19 m for manual measurements in Gohyaku River. Similarly, in Sakura River, these values were 0.18 m and 0.17 m, respectively. Generally, the G3Point program accurately estimates the length of the b-axis. For the a-axis length, the cumulative curves of automated and manual measurements were similar in the regions below the 50th percentile. However, they diverge in the larger grain size regions, indicating that the automated measurements are generally accurate except for larger cobbles and boulders. The automated measurements erroneously overestimate the c-axis of gravels (Fig. 7 (b), (d)). Nevertheless, the median grain size measured by the fitting of ellipsoids using G3Point differed by only 0.02 m from the manual measurement results.

5.3.2 Grain size distribution

Spatial distributions of grain size along river channels were examined from the D_{50} values obtained in measured points (Fig. 8). The median grain diameters of riverbed gravels in the study area ranged from 0.4 to 0.7 m. Fukazawa and Takinosawa exhibited a downstream fining trend, although the spatial variation of the grain size in Takinosawa was much weaker than in Fukazawa. Other tributaries (Hisawa, Sangasawa, Gohyaku River) exhibited constant grain distributions, and thus the change rate α_d in the grain size trend (Eq. 31) was almost zero. As the

https://doi.org/10.5194/egusphere-2025-4283
Preprint. Discussion started: 30 September 2025

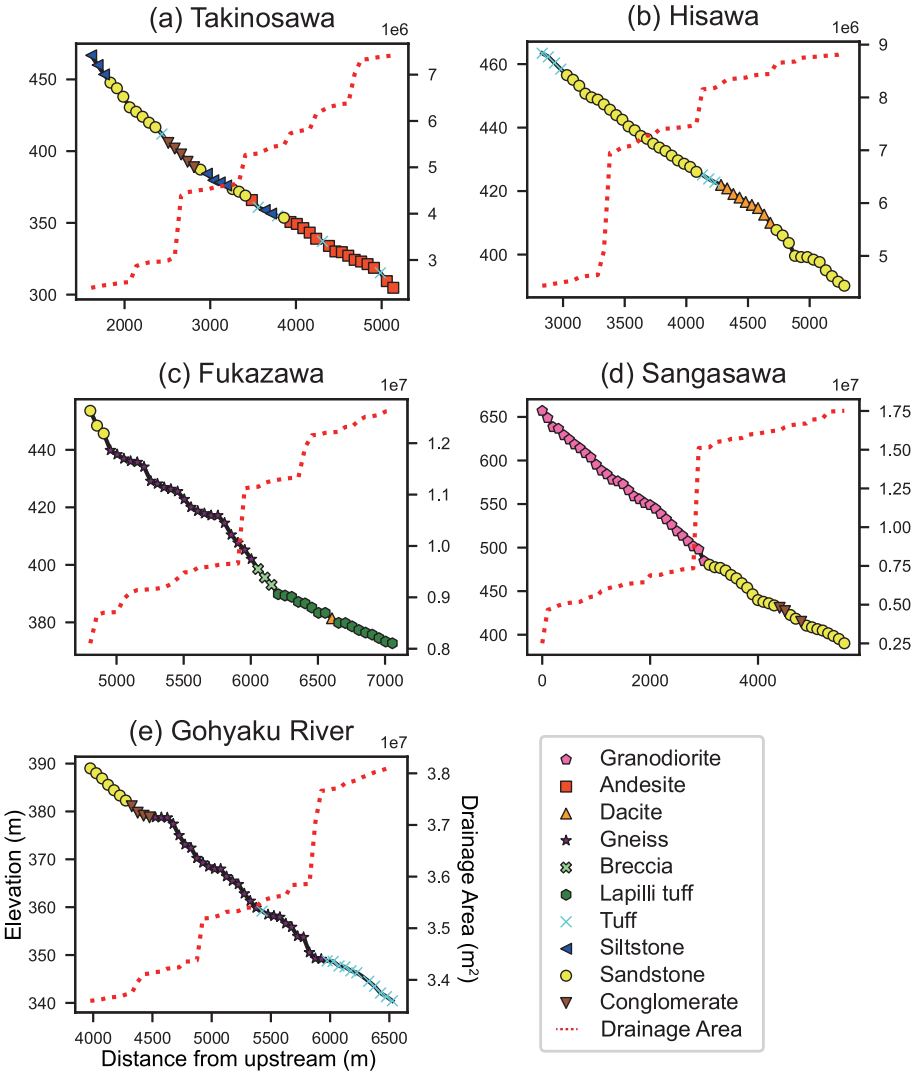

Figure 4. River profiles extracted from the DEM and the lithology data obtained through field surveys—the point on the channel positioned at 10-m intervals. The upstream end was at the channel's endpoint on the map.

https://doi.org/10.5194/egusphere-2025-4283
Preprint. Discussion started: 30 September 2025

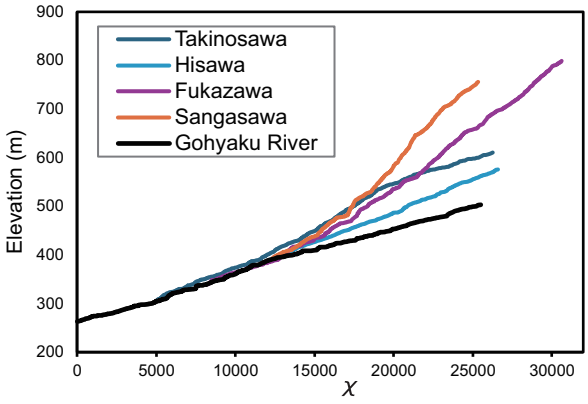

Figure 5. Channel profiles represented by the chi plot. The x-axis represents chi calculated by Eq. (29). In this study, the concavity m/n was assumed to be 0.36 to draw the chi plot.

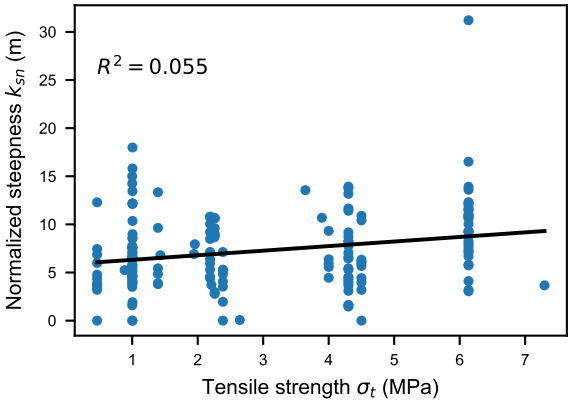

Figure 6. The relationship between normalized steepness and bedrock tensile strengths. Rock tensile strength is weakly correlated with the river steepness.

https://doi.org/10.5194/egusphere-2025-4283
Preprint. Discussion started: 30 September 2025

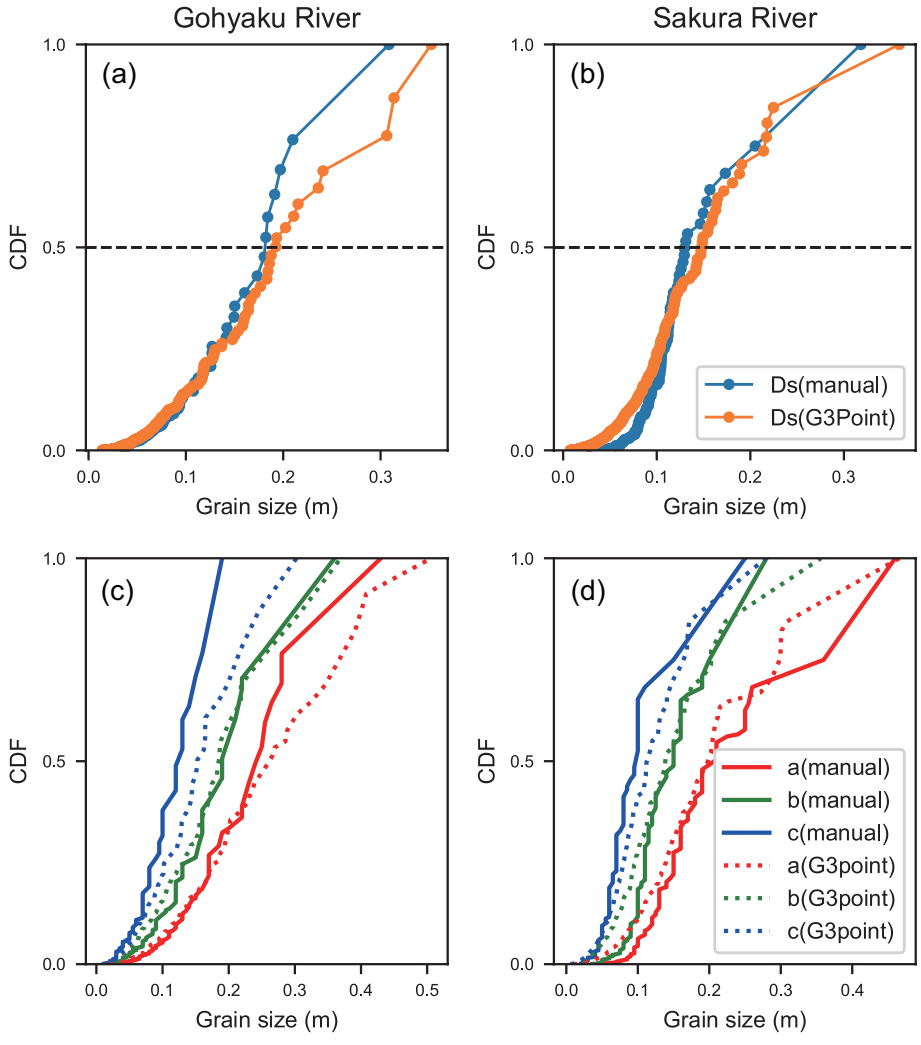

Figure 7. Comparison between automated (G3Point) and manual grain size measurements. The curves represent cumulative distribution functions (CDF), with the vertical axis indicating cumulative volume (%). Orange plots show grain size data obtained using G3Point, while blue plots represent manually measured data. The dashed line indicates the median grain size (D_{50}). The D_{50} value derived from G3Point was slightly larger than that from manual measurements, with a difference of approximately 0.02 m.

https://doi.org/10.5194/egusphere-2025-4283
Preprint. Discussion started: 30 September 2025

Table 3. Measured rock tensile strength σ_t measured in this study. The asterisk mark ($*$) indicates that the tensile strength values were not measured at the tributary, and the values were substituted by those measured in other tributaries.

Rock type	Location	σ_t [MPa]
Granodiorite	Sangasawa	6.1
Dacite	Hisawa	6.3
	Fukazawa	8.2
Andesite	Takinosawa	4.5
Gneiss	Fukazawa, Gohyaku River	4.3
Breccia	Fukazawa	0.5*
Lapilli tuff	Fukazawa	2.4
Tuff	Takinosawa	0.5
	Fukazawa	0.4
	Hisawa, Gohyaku River	0.4*
Conglomerate	Takinosawa	2.3
	Gohyaku River	1.3
	Sangasawa	1.3*
Sandstone	Takinosawa	2.2
	Hisawa	0.4
	Fukazawa	1.0
	Sangasawa	1.0*
Siltstone	Takinosawa	1.4

median grain diameter decreases, the grain size variation also tended to decrease. In general, grain distribution becomes discontinuous at the point of the check dam, but these grain distribution results did not consider the dams for simplicity.

5.4 Model predictions for bedrock river profiles

The numerical experiments using the sediment-flux-dependent well reproduced the actual river profiles. The channel width coefficient k_w, which was optimized for the calculation, ranged from 1.0 to 2.1, and the optimized value for the discharge coefficient k was 117.2. Using optimized k_w, k, and Eq. (18), channel width becomes 5 m – 9 m at Takinosawa, 5 m – 7 m at Hisawa, 13 m – 16 m at Fukazawa, 4 m – 9 m at Sangasawa, and 22 m – 24 m at Gohyaku River.

The observed and modeled river slopes exhibited consistently smooth profiles, regardless of underlying bedrock strength (Fig. 9). The mean squared error between the SFDM and actual profile was 3.5 m, which was the best among the three models (SFDM, ASPM, and SPACEM) examined in this study. The model prediction for Sangasawa reproduced the knickpoint due to the remarkable change in drainage area. Takinosawa had a concave-upward profile, and the model simulated a similar profile due to the downstream fining grain size distribution. However, the model failed to reconstruct the step-like structures observed in Fukazawa and Gohyaku Rivers. This discrepancy was

https://doi.org/10.5194/egusphere-2025-4283
Preprint. Discussion started: 30 September 2025

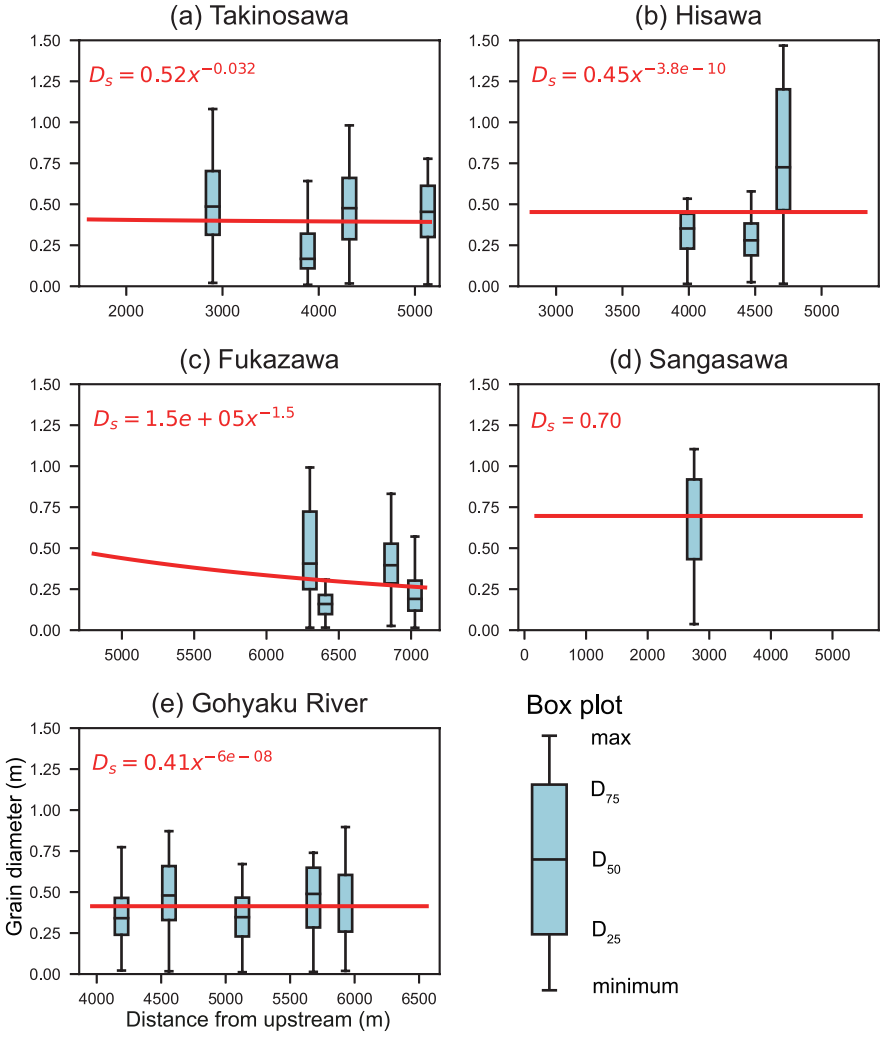

Figure 8. Measured results of grain size distributions for each tributary. Blue box plots represent the median and quantile ranges of the grain diameter. The red line represents the estimated spatial distribution of D_{50}.

https://doi.org/10.5194/egusphere-2025-4283
Preprint. Discussion started: 30 September 2025

Table 4. Input parameters of the sediment-flux-dependent model.

Input parameters	SFDM	params	ASPM	SPACEM
Uplift rate U	375 m Myr^{-1}	Uplift rate	375 m Myr^{-1}	375 m Myr^{-1}
Erosional efficiency β_0	0.0001	Erosional coefficient k_a	5.8	–
Average precipitation rate $\bar{P}$	4.07 $\times 10^{-8}$ m s^{-1}	Discharge coefficient k	–	3.1
Grain diameter D_s	0.3 – 0.7 m	Sediment erodibility K_{sed}	–	1.1×0^{-5}
Tensile strength σ_t	0.4 – 8.2 MPa	Lithological erodibility L_E, K_r	0.3 – 1.7	5.3×10^{-8} – 1.0×10^{-5}
Nondimensional critical shear stress τ_c^*	0.004	Drainage area exponent m	0.5	0.75
Bedrock roughness k_b	0.0032	Slope exponent n	1.0	1.5
Discharge coefficient k	120.4	Settling velocity W_s	–	42 m s^{-1}
Channel width coefficient k_w		Bedrock roughness H_*	–	1.0 m
Takinosawa	1.7			
Hisawa	1.1			
Fukazawa	2.2			
Sangasawa	1.0			
Gohyaku River	1.5			

See each value of D_s and σ_t in Fig. 8 and Tab. 3.

particularly pronounced in areas underlain by hard bedrocks such as granodiorite and gneiss. Thus, although the SFDM did not capture fine topographical changes on a scale of a few hundred meters, it accurately reproduced the overall characteristics of the bedrock river profiles.

In contrast to the SDFM, the profiles predicted by the stream power models (ASPM and SPACEM) did not agree with the actual profiles. Their predictions reflected the bedrock strengths clearly in slopes (Fig. 10). The optimized erosional coefficient for ASPM k_a was 5.8 [yr^{-1}], and the optimized discharge coefficient k for SPACEM was 3.0. The ASPM profile exhibited a remarkable change in slope at the lithologic boundary of the river bedrocks. Especially in Sangasawa, where the contrast in bedrock strength was most pronounced, the ASPM predicted upstream steepness distributed in granodiorite was 9 times steeper than downstream steepness distributed in sandstone. The actual Sangasawa slope change was very small, so that this ASPM result was significantly different from the actual profile (Fig. 10).

The profiles predicted by the SPACEM still deviated from the actual profiles (Figs. 9 and 10), although they were smoother than those of the ASPM. In Sangasawa, the modeled slope of SPACEM changed at the lithological boundary, with the upstream slope being about four times steeper than the downstream slope. The mean squared error between the ASPM and the actual profiles was 21.7, and that of the SPACEM was 13.2.

https://doi.org/10.5194/egusphere-2025-4283
Preprint. Discussion started: 30 September 2025

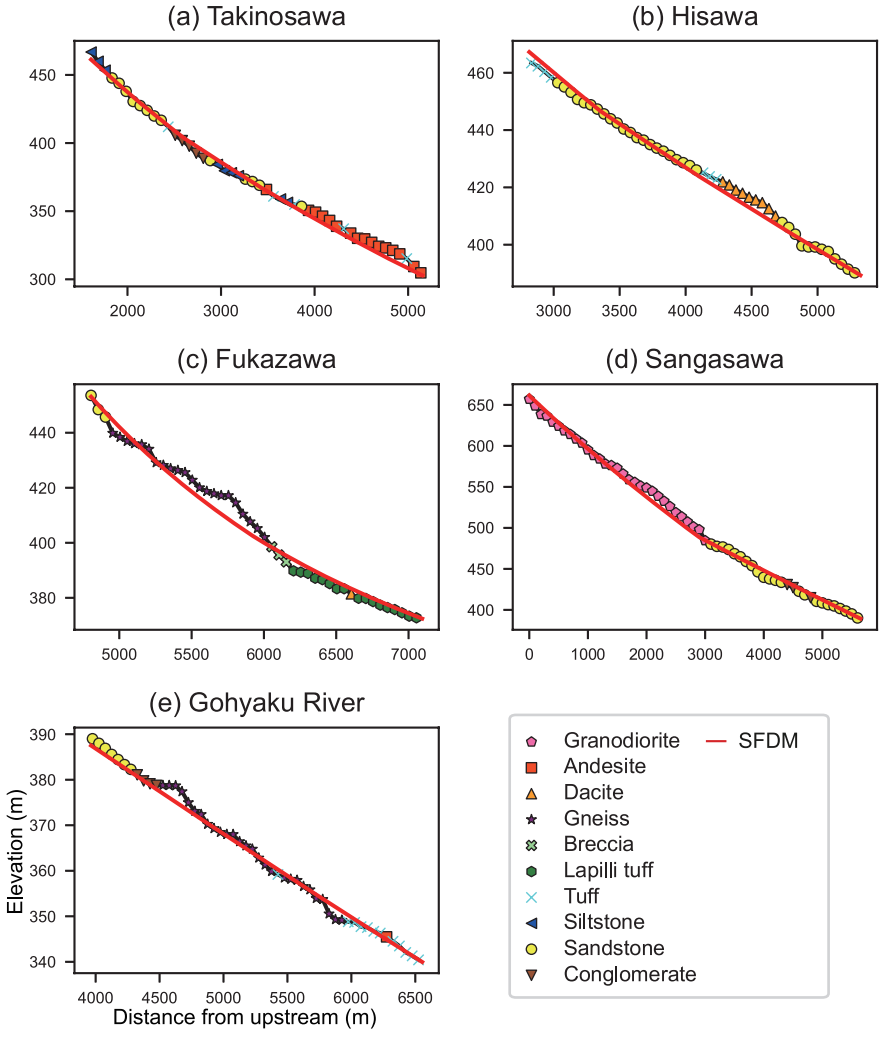

Figure 9. Results of reproduction of the river longitudinal profiles using a sediment-flux-dependent model. The model was calculated on a 10-meter interval grid under the condition that the erosion and the uplift rates are balanced (steady state). The red line represents the steady-state model profile. The colored plots represent the actual river profiles and lithologies.

https://doi.org/10.5194/egusphere-2025-4283
Preprint. Discussion started: 30 September 2025

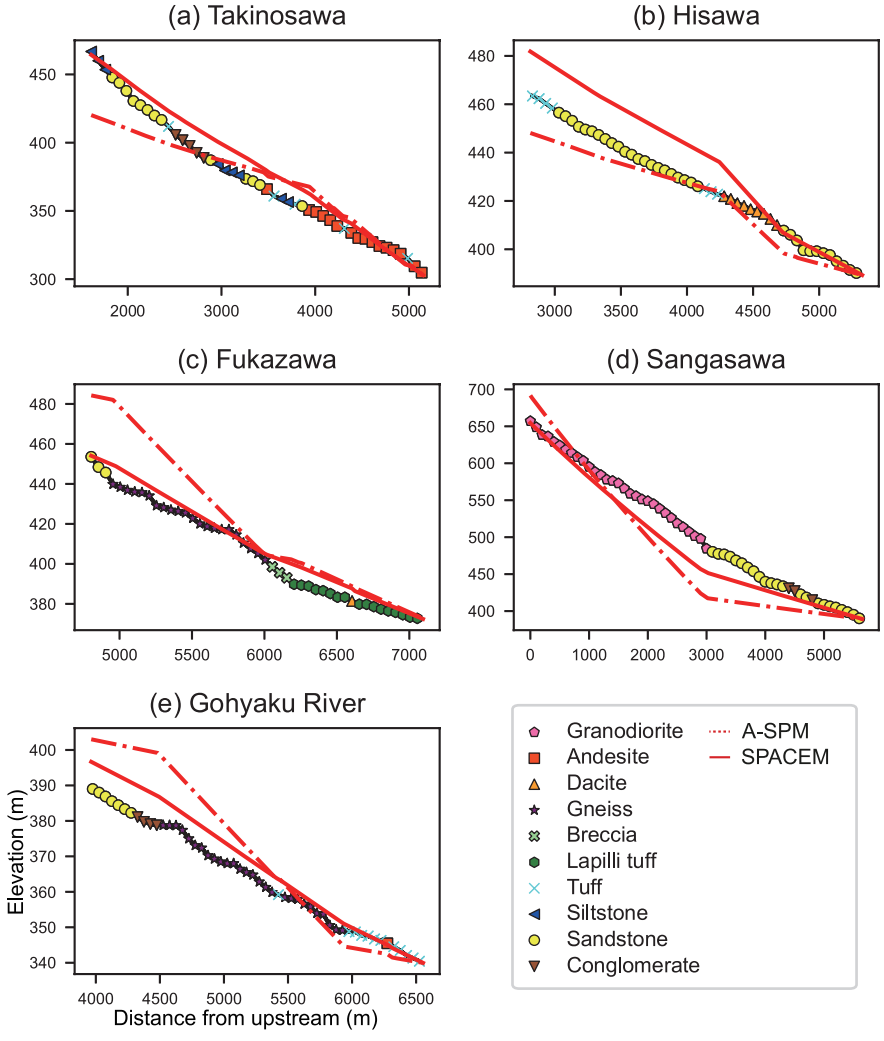

Figure 10. The result of the calculation by ASPM and SPACEM. The red line represents the steady-state profile calculated by SPACEM, and the dashed red line represents that by ASPM. The models were calculated on a 10-meter interval grid, the same as SFDM.

https://doi.org/10.5194/egusphere-2025-4283
Preprint. Discussion started: 30 September 2025

6 Discussion

6.1 Why bedrock strength has little influence on local slopes in river longitudinal profile

The field measurements in this study indicated that the bedrock strength has a limited influence on the river longitudinal profiles. Hayakawa and Oguchi (2009), Brocard et al. (2015), and Takahashi (2025) also suggested that the influence of lithological erodibility on the river profile was small. This study proved this fact clearly by measuring bedrock tensile strength.

The numerical experiments implied that these smooth river profiles over different lithologies are attained by the sediment covering effect (Fig. 11). The sediment-flux-dependent model predicted that the sediment cover ratio mitigated the effect of bedrock strength. Through the cover ratio being higher in soft rocks and lower in hard rocks, erosion is suppressed in soft rock areas, and erosion is promoted in hard rock areas. Eq. (19) indicates that the bedrock strength appears only in the denominator of the first term on the right-hand side of the equation. However, in this equation, the product of the square root of hydraulic roughness $k_s^{1/2}$, the squared rock tensile strength σ_t^2, and the uplift rate U (375 m Myr^{-1} in this study) has a value in the range the order of 10^{-11} to 10^{-13} [kg^{2}m$^{-1/2}$s^{-5}], while the term of the product of coefficient β_0, the grain size $D_s^{1/2}$, and sediment supply rate q_s is the order of 10^{-10} [kg^{2}m$^{-1/2}$s^{-5}]. Thus, it is clear from the equation that the value of rock tensile strength has little effect on the resulting slope. The mechanical explanation for controlling the sediment cover ratio in relation to lithology is as follows.

Considering the cover ratio, even minor changes in river slope can substantially alter erosion rates, effectively mitigating the influence of the bedrock strength. The sediment cover ratio on the bedrock surface increases as the sediment transport capacity approaches the actual sediment supply. Conversely, the cover ratio P_c decreases when the sediment supply is limited or when transport capacity increases. This dynamics is explicitly considered in the sediment-flux-dependent model, in which P_c is formulated as the ratio of sediment supply q_s to the transport capacity q_t (Sklar and Dietrich, 2004; Chatanantavet and Parker, 2009). Here, the sediment supply is primarily governed by upstream conditions, while the transport capacity q_t is controlled by the bed shear stress, which increases with the channel slope S. Therefore, under constant sediment supply, the cover ratio P_c is slope-dependent (Fig. 11). This dependence is particularly pronounced at low gradients, where the bed shear stress is near the threshold for the gravel mobilization, making P_c highly sensitive to small changes in slope (Fig. 12). Because the sediment cover shields the bedrock from direct impact by bedload particles, even slight variations in slope—and thus in cover ratio—can lead to significant differences in erosion rates.

As a result, river longitudinal profiles tend not to exhibit marked changes across lithologic boundaries unless the slope becomes exceptionally steep. Although channel gradients over resistant lithologies are marginally steeper than those over weaker ones, the difference is often too subtle to be discerned either in numerical simulations or natural river profiles (Figs. 6, 9, and 11). This finding aligns with previous studies. Sklar and Dietrich (2006) demonstrated that the rock strength exerts only a limited influence on channel profiles in models that incorporate the sediment cover effect. Similarly, Guryan et al. (2024) showed that the variability in channel slope due to differences in rock erodibility is smoothed out when sediment cover dynamics are included in numerical simulations. The present study further supports these findings by demonstrating, through numerical experiments using field-derived datasets, that sediment cover effectively offsets the influence of bedrock strength on river profile morphology.

This study proposes that the relationship between the cover ratio and river slope is a critical factor, and the SFDM well reproduces this relationship. The ASPM does not consider the sediment cover ratio, and therefore, it fails to predict the actual river longitudinal profiles. While the SPACEM (Guryan et al., 2024) also considers the cover ratio, its reproducibility is inferior to that of the SFDM (Figs. 9 and 10). The reason for this discrepancy lies in the formulation of the relationship between cover ratio P_c and channel slope S in the SPACEM. Figure 12 (a), (b) illustrates cover ratio and erosional rates against slopes for both SPACEM and SFDM. Both models assume that the

https://doi.org/10.5194/egusphere-2025-4283
Preprint. Discussion started: 30 September 2025

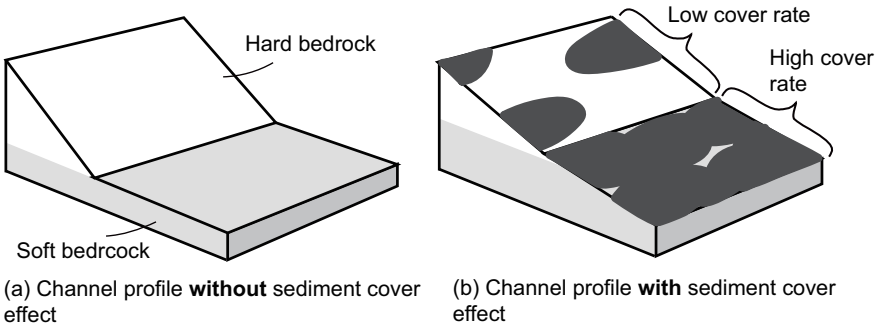

Figure 11. Comparison of channel profiles across two lithologies with and without sediment cover. (a) Without sediment cover. (b) With sediment cover.

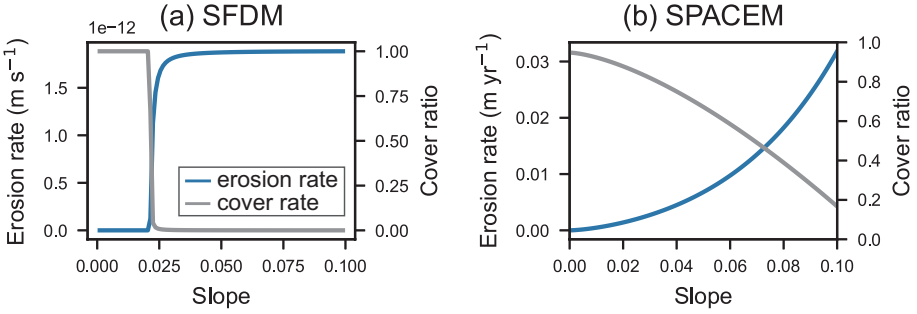

Figure 12. Changes in erosion rate and sediment cover ratio with slope in SFDM and SPACEM. The blue line represents changes in erosion rate, while the gray line indicates changes in sediment cover ratio. (a) SFDM result. Erosion rate and cover ratio change rapidly in a specific region of the slope. (b) SPACEM result. Both erosion rate and cover ratio change gently.

erosional rate is proportional to the ratio of bedrock exposure. In the case of SFDM, the bedrock exposure ratio is defined as $1 - P_c$. In contrast, SPACEM adopts the log-scale definition e^{-H/H_*} , resulting in a weaker topographic response to variations in the ratio of sediment cover. At present, the former formulation is more suitable for representing actual river profiles. However, there is no physical basis to suggest that the cover ratio is linearly correlated with the sediment supply/transport capacity ratio; therefore, further investigation is necessary to improve the cover (or exposure) ratio to better fit real-world conditions in future research.

It is important to note that the present study focuses primarily on rivers that have approached a state of equilibrium between uplift and erosion. In contrast, rivers that are far from equilibrium conditions often exhibit distinctly steep channel gradients, characterized by prominent knickpoints propagating upstream. Around such knickpoints, sediment cover typically becomes minimal or absent, drastically reducing the buffering effect of sediment cover on rock erosion. Consequently, under disequilibrium conditions, differences in rock erodibility can more directly impact the shape of river longitudinal profiles.

https://doi.org/10.5194/egusphere-2025-4283
Preprint. Discussion started: 30 September 2025

6.2 Lithologic controls for river longitudinal profiles

Although bedrock strength may not directly control local channel gradients, lithology can still exert an indirect influence on the entire morphology of channel longitudinal profiles by shaping the grain size distribution and sediment flux. As shown in Eq. (19), the primary factors determining channel profiles are the water discharge per unit width q_w, grain size D_s, and sediment flux q_s. Among these, the latter two parameters are potentially regulated by the lithologic characteristics of the upstream drainage areas.

Grain size distributions of sediment are known to vary significantly depending on the lithology of their drainage basins (Kodama, 1994; Sklar et al., 2017; Roda-Boluda et al., 2018; Verdian et al., 2021; Takahashi, 2025). Sediment grains are initially produced on hillslopes through physical and chemical weathering processes, where lithology, along with tectonics and climate, plays a critical role in determining grain sizes (Sklar, 2024). Field measurements have consistently highlighted the importance of lithology, owing to its control on the physical and chemical properties of parent rocks, in influencing grain size distribution. For instance, (Sklar et al., 2017) demonstrated a clear correlation between rock strength and the sizes of rock fragments measured in soils in California. Similarly, (Verdian et al., 2021) conducted field measurements of clast sizes, indicating that gravels derived from massive granitic plutons exhibited the largest, those from surficial basalt flows had intermediate sizes, and those from marine ribbon chert were the smallest. Collectively, these studies underscore the significant control exerted by hillslope lithology on grain size.

Bedrock lithology in hillslope regions also controls the ratio of bedloads to the eroded materials (Chatanantavet and Parker, 2009), which affects the sediment flux q_s provided to streams. The sediment supply rate depends on the erosional rate, the drainage area, and the mode of mechanical weathering that determines the ratio of bedload materials in sediment (Eq. (16)). For example, (Roda-Boluda et al., 2018) examined the frequency and size of landslides in southern Italy, focusing on their relationship with the local slope steepness and rock strength. They discovered that the frequency of landslides increases as the slope is composed of softer rock, which promotes the larger sediment production rates.

Thus, the lithologic composition of bedrock across the drainage basin from hill slopes to fluvial zones can play a critical role in determining the overall longitudinal profile of river channels. Supporting this notion, the field-based analysis by Takahashi (2025) in the Tsugaru region of Japan demonstrated that variations in channel morphology are strongly linked to differences in sediment load and grain size, both of which are influenced by upstream lithology. The findings of this study are consistent with this interpretation. The bedrock types in the hillslope regions of the studied tributaries can be broadly divided into two categories: granodiorites and sedimentary rocks. Granodioritic bedrocks are predominantly exposed in the upstream catchments of Fukazawa and Sangasawa, whereas sedimentary rocks dominate the upstream areas of Takinosawa, Hisawa, and Gohyku River (Kubo et al., 2003; Yamamoto and Sakaguchi, 2023). Chi-plots analysis (Fig. 5) revealed that the channel steepness indices of Fukazawa and Sangasawa tended to be notably higher in their upper reaches compared to the other tributaries. This pattern suggests that upstream lithology— specifically, the presence of more resistant granodiorite—may enhance channel steepness by influencing sediment grain size and transport rates. These observations underscore the indirect yet significant role of lithologic variation in controlling longitudinal channel profile. Further quantitative predictions of such lithologic controls remain a key challenge for future research.

7 Conclusion

To investigate the influence of bedrock strength on fluvial morphology, this study combined field surveys with numerical experiments. The results revealed that the sediment cover effect plays a key role in mitigating the impact of variations in bedrock erodibility on river profile morphology.

https://doi.org/10.5194/egusphere-2025-4283
Preprint. Discussion started: 30 September 2025

Field surveys were conducted in the Abukuma River basin in northeastern Japan, where tributaries incise bedrock of varying lithologies exposed in close proximity. Bedrock strength and riverbed gravel grain size distributions were measured in each tributary. Tensile strength of bedrock samples, obtained through the Brazilian splitting test, varied by more than an order of magnitude. Despite this, no significant differences were observed in the channel slopes across the longitudinal profiles of these rivers (Fig. 6).

To explain the apparent insensitivity of river longitudinal profiles to local variations in bedrock strength, we carried out numerical experiments using three models that account for bedrock erodibility to different extents: the sediment-flux-dependent model (SFDM), the area-based stream power model (ASPM), and the stream power with alluvium conservation and entrainment model (SPACEM). All three incorporate bedrock erodibility, while SFDM and SPACEM also include the effects of sediment cover. Among them, only SFDM explicitly incorporates the sediment tool effect, which describes the enhanced erosion by mobile sediment particles.

The SFDM simulations demonstrated that the sediment cover effect buffers the influence of rock erodibility on channel slope. In regions with high bedrock erodibility, increased erosion tends to lower channel gradients. This reduction in slope, in turn, reduces sediment transport capacity, leading to greater sediment cover. The increased cover inhibits further erosion by reducing the sediment tool effect, establishing a negative feedback loop. This mechanism effectively dampens variations in slope, even in the presence of substantial differences in bedrock strength.

The numerical results emphasize the importance of incorporating both sediment cover and the sediment tool effect when evaluating the geomorphic consequences of bedrock erodibility. Among the three models, SFDM most accurately reproduced the observed longitudinal river profiles, exhibiting little to no slope variation in areas of differing lithology. In contrast, ASPM, which does not consider sediment cover, predicted prominent slope breaks inconsistent with field observations. SPACEM performed better by including sediment cover, but still exhibited unrealistic local slope variations, as it lacks explicit treatment of the sediment tool effect.

While bedrock strength does not directly control local channel gradients, this study suggests that upstream lithology can indirectly influence overall channel steepness by modifying sediment grain size and supply rates. Future research should aim to incorporate more extensive datasets on gravel characteristics to better quantify this indirect relationship between bedrock properties and fluvial morphology.

8 Notation

a	the ratio of the bedload to the total sediment supply.
A	drainage area (m^2).
A_0	a reference drainage area (m^2).
C_f	a friction coefficient.
D	a diameter of the specimen (m).
D_s	grain diameter (m).
E	erosion rate ($m\ s^{-1}$).
E_{eq}	erosion rate in steady state ($m\ s^{-1}$).
E_r	erosion rate in SPACEM ($m\ yr^{-1}$).
E_s	rate of entraintment in SPACEM ($m\ yr^{-1}$).
g	acceleration of gravity ($m\ s^{-2}$).
H	thickness of sediment cover (m).
H_*	bedrock roughness scale (m).

https://doi.org/10.5194/egusphere-2025-4283
Preprint. Discussion started: 30 September 2025

I_r	rate of particle impacts per unit area per unit time.
k	discharge coefficient.
k_a	erosional coefficient (L^{1-2m} T^{-1}).
k_s	hydraulic roughness height (m).
k_{sn}	normalized steepness.
k_v	rock resistance coefficient.
k_w	channel width coefficient.
K_r	bedrock erodibility (L^{1-2m} T^{-1}).
$K_{r,i}$	the ith rock type erodibility.
K_{sed}	sediment erodibility.
L	length of the specimen (m).
L_E	relative lithological erodibility index.
L_s	saltation hop length (m).
m	a drainage area exponent in stream power models.
M_p	particle mass (kg).
n	a slope exponent in stream power models.
$\bar{P}$	average precipitation rate (m^2 s^{-1}).
P_c	cover ratio.
P_{max}	maximum load (kN).
q	water discharge per unit width (m^2 s^{-1}).
q_s	sediment flux volume per unit width (m^2 s^{-1}).
q_t	sediment transport capacity per unit width (m^2 s^{-1}).
Q_w	water discharge (m^3 s^{-1}).
R_b	nondimensional buoyant density of sediment.
S	channel slope.
U	uplift rate (m s^{-1}).
U_i	particle impacr velocity (m s^{-1}).
V_i	average volume eroded per particle impact.
w_{si}	vertical sediment velocity on impact (m s^{-1}).
W	channel width (m).
W_s	settling velocity (m s^{-1}).
x	distance along the channel from upstream (m).
Y	Young's modulus (MPa).
α	saltation impact angle.
α_d	change rate of the grain diameter.
β_0	an empirical erosional coefficient.
ε_v	unit volume detachment energy (J m^{-3}).
η	bedrock elevation (m).

https://doi.org/10.5194/egusphere-2025-4283
Preprint. Discussion started: 30 September 2025

θ	channel concavity index.
κ_a	roughness coefficient linear to the grain size (m).
κ_b	bedrock roughness (m).
ρ_s	sediment density (kg m^{-3}).
ρ_w	water density (kg m^{-3}).
σ_t	bedrock tensile strength (MPa).
$\sigma_{t,i}$	tensile strengths of the ith rock type (MPa).
$\sigma_{\mathrm{t,tuff}}$	tensile strength of tuff (MPa).
τ_b	bed shear stress (Pa).
τ^*	nondimensional bed shear stress.
τ_c^*	nondimentional critical shear stress.
ϕ	sediment porocity.

Code and data availability. All data and code supporting this study are openly available on Zenodo. Bedrock strength dataset: available at Zenodo, DOI: 10.5281/zenodo.17017130. Grain size analysis dataset: available at Zenodo, DOI: 10.5281/zenodo.17017613. River incision model calculation code and outputs: available at Zenodo, DOI: 10.5281/zenodo.17017800. DEM data were obtained from the Geospatial Information Authority of Japan, which are available via their web portal.

Author contributions. N.Y. and H.N. designed research; N.Y. performed research; N.Y. analyzed data; and N.Y and H.N. wrote the paper.

Competing interests. The authors declare no competing interest.

Acknowledgements. This work was supported by JSPS KAKENHI Grant Number 23K22872 and Sediment Dynamics Research Consortium (sponsored by INPEX, JAPEX, and JOGMEC). The authors used ChatGPT and Grammarly to enhance the clarity and readability of the manuscript during its preparation.

https://doi.org/10.5194/egusphere-2025-4283
Preprint. Discussion started: 30 September 2025

References

Aubert, G., Langlois, V. J., and Allemand, P.: Bedrock incision by bedload: insights from direct numerical simulations, Earth Surface Dynamics, 4, 327–342, https://doi.org/10.5194/esurf-4-327-2016, 2016.

Bao, T., Hashiba, K., and Fukui, K.: Effect of Water Saturation on the Brazilian Tension Test of Rocks, MATERIALS TRANSACTIONS, 62, 48–56, https://doi.org/10.2320/matertrans.M-M2020857, 2021.

Beer, A. R., Turowski, J. M., and Kirchner, J. W.: Spatial patterns of erosion in a bedrock gorge, Journal of Geophysical Research: Earth Surface, 122, 191–214, https://doi.org/https://doi.org/10.1002/2016JF003850, 2017.

Bitter, J. G. A.: A study of erosion phenomena part I, Wear, 6, 5–21, https://doi.org/https://doi.org/10.1016/0043-1648(63)90003-6, 1963.

Brocard, G. Y., Willenbring, J. K., Scatena, F. N., and Johnson, A. H.: Effects of a tectonically-triggered wave of incision on riverine exports and soil mineralogy in the Luquillo Mountains of Puerto Rico, Applied Geochemistry, 63, p. 586–598, https://doi.org/10.1016/j.apgeochem.2015.04.001, 2015.

Campforts, B., Vanacker, V., Herman, F., Vanmaercke, M., Schwanghart, W., Tenorio, G. E., Willems, P., and Govers, G.: Parameterization of river incision models requires accounting for environmental heterogeneity: insights from the tropical Andes, Earth Surface Dynamics, 8, 447–470, https://doi.org/10.5194/esurf-8-447-2020, 2020.

Carr, J., DiBiase, R., Yeh, E., Fisher, D., and Kirby, E.: Rock properties and sediment caliber govern bedrock river morphology across the Taiwan Central Range, Science Advances, 9, https://doi.org/10.1126/sciadv.adg6794, publisher Copyright: Copyright © 2023 The Authors, some rights reserved;, 2023.

Chatanantavet, P. and Parker, G.: Physically based modeling of bedrock incision by abrasion, plucking, and macroabrasion, Journal of Geophysical Research Atmospheres, 114, https://doi.org/10.1029/2008JF001044, 2009.

Conrad, O., B. B. B. M. D. H. F. E. G. L. W. J. W. V. and Böhner, J.: System for Automated Geoscientific Analyses (SAGA) v. 2.1.4, 8, https://doi.org/10.5194/gmd-8-1991-2015, 2015.

Engle, P. A.: Impact Wear of Materials, Elsevier Sci., New York, 1978.

Fernández, R., Parker, G., and Stark, C. P.: Experiments on patterns of alluvial cover and bedrock erosion in a meandering channel, Earth Surface Dynamics, 7, 949–968, https://doi.org/10.5194/esurf-7-949-2019, 2019.

Finnegan, N. J., Roe, G., Montgomery, D. R., and Hallet, B.: Controls on the channel width of rivers: Implications for modeling fluvial incision of bedrock, Geology, 33, 229–232, https://doi.org/10.1130/G21171.1, 2005.

Fujiwara, O., Yanagida, M., and Sanga, T.: Late Pleistocene to Holocene Vertical Displacement Rates in Japanese Islands, The Earth Monthly, 26, 442–447, 2004.

Fujiwara, O., Makoto, Y., Sanga, T., and Moriya, T.: Researches on tectonic uplift and denudation with relation to geological disposal of HLW in Japan, Nuclear Fuel Cycle and Environment, 11, 113–124, https://doi.org/10.3327/jnuce.11.113, 2005.

Fukuda, S., Sueoka, S., Kohn, B. P., and Tagami, T.: (U–Th)/He thermochronometric mapping across the Northeast Japan Arc: towards understanding mountain building in an island-arc setting, Earth, Planets and Space, 72, https://doi.org/https://doi.org/10.1186/s40623-020-01151-z, 2020.

Guryan, G. J., Johnson, J. P. L., and Gasparini, N. M.: Sediment Cover Modulates Landscape Erosion Patterns and Channel Steepness in Layered Rocks: Insights From the SPACE Model, Journal of Geophysical Research: Earth Surface, 129, e2023JF007 509, https://doi.org/https://doi.org/10.1029/2023JF007509, e2023JF007509 2023JF007509, 2024.

https://doi.org/10.5194/egusphere-2025-4283
Preprint. Discussion started: 30 September 2025

Haag, M. B., Schoenbohm, L. M., Wolpert, J., Jess, S., Bierman, P., Corbett, L., Sommer, C. A., and Endrizzi, G.: Rock strength controls erosion in tectonically dead landscapes, Science Advances, 11, eadr2610, https://doi.org/10.1126/sciadv.adr2610, 2025.

Hayakawa, Y. S. and Oguchi, T.: GIS analysis of fluvial knickzone distribution in Japanese mountain watersheds, Geomorphology, 111, 27–37, https://doi.org/https://doi.org/10.1016/j.geomorph.2007.11.016, gIS and SDA applications in geomorphology, 2009.

Howard, A. D.: A detachment-limited model of drainage basin evolution, Water Resources Research, 30, 2261–2285, https://doi.org/https://doi.org/10.1029/94WR00757, 1994.

Ichikawa, K.: Pre-Cretaceous terranes of Japan, publication of IGCP Project No. 224, Pre-Jurassic evolution of Eastern Asia, 1990.

Inoue, T., Izumi, N., Shimizu, Y., and Parker, G.: Interaction among alluvial cover, bed roughness, and incision rate in purely bedrock and alluvial-bedrock channel, Journal of Geophysical Research: Earth Surface, 119, 2123–2146, https://doi.org/https://doi.org/10.1002/2014JF003133, 2014.

Inoue, T., Yamaguchi, S., and Nelson, J. M.: The effect of wet-dry weathering on the rate of bedrock river channel erosion by saltating gravel, Geomorphology, 285, 152–161, https://doi.org/https://doi.org/10.1016/j.geomorph.2017.02.018, 2017.

Johnson, J., Whipple, K., Sklar, L., and Hanks, T.: Transport slopes, sediment cover, and bedrock channel incision in the Henry Mountains, Utah, J. Geophys. Res, 114, https://doi.org/10.1029/2007JF000862, 2009.

Kodama, Y.: Downstream changes in the lithology and grain size of fluvial gravels, the Watarase River, Japan; evidence of the role of abrasion in downstream fining, Journal of Sedimentary Research, 64, 68–75, https://doi.org/10.1306/D4267D0C-2B26-11D7-8648000102C1865D, 1994.

Kubo, K., Yanagisawa, Y., Yamamoto, T., Komazawa, M., Hiroshima, T., and Sudou, S.: Geological Map, 1:200,000, Fukushima, Tech. Rep. NJ-54-16,22, Geological survey of Japan, AIST, 2003.

Luque, R. F. and and, R. V. B.: Erosion And Transport Of Bed-Load Sediment, Journal of Hydraulic Research, 14, 127–144, https://doi.org/10.1080/00221687609499677, 1976.

Matsushi, Y., Matsuzaki, H., and Makino, H.: Testing Models of Landform Evolution by Determining the Denudation Rates of Mountainous Watersheds using Terrestrial Cosmogenic Nuclides, Japanese Geomorphological Union, 35, 165–185, https://cir.nii.ac.jp/crid/1520290882637797888, 2014.

Molnar, P. and England, P.: Late Cenozoic uplift of mountain ranges and global climate change: chicken or egg?, 346, 29–34, https://doi.org/https://doi.org/10.1038/346029a0, 1990.

O'Callaghan, J. F. and Mark, D. M.: The extraction of drainage networks from digital elevation data, Computer Vision, Graphics, and Image Processing, 28, 323–344, https://doi.org/https://doi.org/10.1016/S0734-189X(84)80011-0, 1984.

Perron, J. T. and Royden, L.: An integral approach to bedrock river profile analysis, Earth Surface Processes and Landforms, 38, 570–576, https://doi.org/https://doi.org/10.1002/esp.3302, 2013.

Pritchard, D., Roberts, G., White, N., and Richardson, C.: Uplift histories from river profiles, Geophysical Research Letters, 36, https://doi.org/10.1029/2009GL040928, 2009.

Roberts, G. G., White, N. J., Martin-Brandis, G. L., and Crosby, A. G.: An uplift history of the Colorado Plateau and its surroundings from inverse modeling of longitudinal river profiles, Tectonics, 31, https://doi.org/https://doi.org/10.1029/2012TC003107, 2012.

Roda-Boluda, D. C., D'Arcy, M., McDonald, J., and Whittaker, A. C.: Lithological controls on hillslope sediment supply: insights from landslide activity and grain size distributions, Earth Surface Processes and Landforms, 43, 956–977, https://doi.org/https://doi.org/10.1002/esp.4281, 2018.

https://doi.org/10.5194/egusphere-2025-4283
Preprint. Discussion started: 30 September 2025

Sklar, L. and Dietrich, W. E.: River Longitudinal Profiles and Bedrock Incision Models: Stream Power and the Influence of Sediment Supply, pp. 237–260, American Geophysical Union (AGU), ISBN 9781118664292, https://doi.org/https://doi.org/10.1029/GM107p0237, 1998.

Sklar, L. S.: Grain Size in Landscapes, Annual Review of Earth and Planetary Sciences, 52, 663–692, https://doi.org/https://doi.org/10.1146/annurev-earth-052623-075856, 2024.

Sklar, L. S. and Dietrich, W. E.: Sediment and rock strength controls on river incision into bedrock, Geology, 29, 1087–1090, https://doi.org/10.1130/0091-7613(2001)029<1087:SARSCO>2.0.CO;2, 2001.

Sklar, L. S. and Dietrich, W. E.: A mechanistic model for river incision into bedrock by saltating bed load, Water Resources Research, 40, https://doi.org/https://doi.org/10.1029/2003WR002496, 2004.

Sklar, L. S. and Dietrich, W. E.: The role of sediment in controlling steady-state bedrock channel slope: Implications of the saltation abrasion incision model, Geomorphology, 82, 58–83, https://doi.org/10.1016/j.geomorph.2005.08.019, 2006.

Sklar, L. S., Riebe, C. S., Marshall, J. A., Genetti, J., Leclere, S., Lukens, C. L., and Merces, V.: The problem of predicting the size distribution of sediment supplied by hillslopes to rivers, Geomorphology, 277, 31–49, https://doi.org/https://doi.org/10.1016/j.geomorph.2016.05.005, connectivity in Geomorphology from Binghamton 2016, 2017.

Society, T. J. G.: Japanese Geotechnical Society standards : laboratory testing standards of geomaterials, Japan Geotechnical Society and Maruzen Publishing [distributor], https://cir.nii.ac.jp/crid/1130848328362029184, 2016.

Steer, P., Guerit, L., Lague, D., Crave, A., and Gourdon, A.: Size, shape and orientation matter: fast and semi-automatic measurement of grain geometries from 3D point clouds, Earth Surface Dynamics, 10, 1211–1232, https://doi.org/10.5194/esurf-10-1211-2022, 2022.

Sternberg, H.: Untersuchungen über längen-und Querprofil geschiebeführende Flüsse, Zeitschrift für Bauwesen, 25, 483–506, https://cir.nii.ac.jp/crid/1572824500838774016, 1875.

Takahashi, N. O.: Relative role of rock erodibility and sediment load in setting channel slope of mountain rivers, Earth Surface Processes and Landforms, 50, e70 017, https://doi.org/https://doi.org/10.1002/esp.70017, 2025.

Verdian, J. P., Sklar, L. S., Riebe, C. S., and Moore, J. R.: Sediment size on talus slopes correlates with fracture spacing on bedrock cliffs: implications for predicting initial sediment size distributions on hillslopes, Earth Surface Dynamics, 9, 1073–1090, https://doi.org/10.5194/esurf-9-1073-2021, 2021.

Vutukuri, V., Lama, R., and Saluja, S.: Handbook on mechanical properties of rocks. Volume 1: Testing techniques and results, Trans Tech Publishers, 1974.

Whipple, K., DiBiase, R., and Crosby, B.: 9.28 Bedrock Rivers, vol. 9, pp. 550–573, ISBN 9780080885223, https://doi.org/10.1016/B978-0-12-374739-6.00254-2, 2013.

Whipple, K. X.: Bedrock rivers and the geomorphology of active orogens, Annual Review of Earth and Planetary Sciences, 32, 151–185, https://doi.org/10.1146/annurev.earth.32.101802.120356, 2004.

Whipple, K. X. and Tucker, G. E.: Dynamics of the stream-power river incision model: Implications for height limits of mountain ranges, landscape response timescales, and research needs, Journal of Geophysical Research: Solid Earth, 104, 17 661–17 674, https://doi.org/https://doi.org/10.1029/1999JB900120, 1999.

Whipple, K. X. and Tucker, G. E.: Implications of sediment-flux-dependent river incision models for landscape evolution, Journal of Geophysical Research: Solid Earth, 107, ETG 3–1–ETG 3–20, https://doi.org/https://doi.org/10.1029/2000JB000044, 2002.

Wobus, C., Whipple, K. X., Kirby, E., Snyder, N., Johnson, J., Spyropolou, K., Crosby, B., and Sheehan, D.: Tectonics from topography: Procedures, promise, and pitfalls, in: Tectonics, Climate, and Landscape Evolution, Geological Society of America, ISBN 9780813723983, https://doi.org/10.1130/2006.2398(04), 2006.

https://doi.org/10.5194/egusphere-2025-4283
Preprint. Discussion started: 30 September 2025

Yamamoto, T. and Sakaguchi, K.: Geology of the Bandai San District, Tech. Rep. 32, Geological survey of Japan, AIST, 2023.